phys. stat. sol. (b) **238**, No. 3, 568–574 (2003) / **DOI** 10.1002/pssb.200303173

Coherent control of carrier population and spin in (111)-GaAs

Martin J. Stevens[1], **R. D. R. Bhat**[2], **J. E. Sipe**[2], **H. M. van Driel**[2], and **Arthur L. Smirl**[*, 1]

[1] Laboratory for Photonics & Quantum Electronics, 138 IATL, University of Iowa, Iowa City, Iowa 52242, USA
[2] Department of Physics, University of Toronto, 60 St. George Street, Toronto, Ontario M5S 1A7, Canada

Received 14 March 2003, accepted 14 April 2003
Published online 22 July 2003

PACS 42.65.–k, 72.25.Fe

We report independent coherent control of carrier population and spin in (111)-oriented GaAs arising through quantum interference of the transition amplitudes associated with one- and two-photon absorption of ~100 fs phase-locked optical pulses. We demonstrate this coherent control using various combinations of pulse polarizations and crystal orientations. In addition, we present a phenomenological framework for the spin and population control, and present predictions based on a macroscopic symmetry analysis that agree with our experimental observations.

1 Introduction A number of schemes have been implemented that use optical fields to coherently control electron populations in semiconductors. Many of these schemes used one photon absorption of multiple phase-related optical pulses having a single frequency (i.e. a single color) [1–3]. Additionally, circularly polarized light can be used to generate spin-polarized carrier populations in direct-gap semiconductors [4], and in the burgeoning field of "spintronics", optics has played a key role in the injection and study of electron spin [5, 6]. Some of the one-color coherent control schemes have used the polarization of the incident pulses to control carrier spin [1, 2]. There was also a report [7] of using the optical Stark effect to optically manipulate the direction of electron spin, although this latter technique [7] did not rely on the relative optical phase of the pulses.

In addition, *two-color* quantum interference control [8] techniques have been used to control carrier density in semiconductors. By using phase-controlled optical pulses with frequencies ω and 2ω propagating along the [111] direction in bulk GaAs, Fraser et al. showed [8, 9] that carrier population can be coherently controlled through quantum interference between the transition amplitudes associated with single photon absorption of 2ω and two photon absorption of ω connecting the same initial valence band and final conduction band states. However, population control was demonstrated for only one combination of 2ω and ω polarizations [9]. Moreover, in this previous study [9], no spin control was reported.

In this paper, by contrast, we demonstrate all-optical injection and coherent control of both the carrier *population* and the *spin* of the population. We use two-color quantum interference to *independently* control population and spin by systematically varying the phases and polarizations of the two incident pulses and by rotating the sample. In addition, we present a macroscopic symmetry analysis that gives quantitative predictions of both spin and population control for these polarization configurations and sample orientations. We show that these predictions agree with our experimental observations.

2 Phenomenological framework We consider a case in which two optical pulses, with center frequencies ω and 2ω, propagate collinearly and are normally incident on a direct gap semiconductor with band gap energy E_g. The photon energies of these pulses satisfy the relation $\hbar\omega < E_g < \hbar 2\omega$; thus, a carrier

[*] Corresponding author: e-mail: art-smirl@uiowa.edu, Phone: (319) 335-3460, Fax: (319) 335-3462

population (n) can be injected into this semiconductor through one-photon absorption of the 2ω beam ($n_{2\omega}$) or through two photon absorption of the ω beam (n_ω). In addition, carriers can be generated through the quantum mechanical interference between the probability transition amplitudes associated with one- and two-photon absorption (n_I). The total population injection rate can be written [9]:

$$\dot{n} = \dot{n}_{2\omega} + \dot{n}_{\omega} + \dot{n}_{I} \,. \tag{1}$$

Here $\dot{n}_{2\omega} = \sum_{ij} \xi_1^{ij} E_{2\omega}^{i*} E_{2\omega}^{j}$ and $\dot{n}_{\omega} = \sum_{ijkl} \xi_2^{ijkl} E_{\omega}^{i*} E_{\omega}^{j*} E_{\omega}^{k} E_{\omega}^{l}$, where the electric field is written as $\boldsymbol{E}(t) = \boldsymbol{E}_{\omega} \exp(-i\omega t) + \boldsymbol{E}_{2\omega} \exp(-i2\omega t) + \text{c.c.}$, and i, j, k, l are dummy indices representing Cartesian components of the fields corresponding to the crystallographic principle axes [100], [010] and [001]. These are variations on the well-known forms of $n_{2\omega}$ and n_ω from linear and nonlinear optics, where the tensor ξ_1 is related to $\chi^{(1)}$ and describes one photon absorption, and ξ_2 is related to $\chi^{(3)}$ and describes two photon absorption. The interference, or *population control*, component of the total carrier density is

$$\dot{n}_I = \sum_{ijk} \xi_I^{ijk} E_{\omega}^{i*} E_{\omega}^{j*} E_{2\omega}^{k} + \text{c.c.} \,, \tag{2}$$

where the ξ_I tensor is related to the imaginary part of $\chi^{(2)}$ [9]. It has only one independent component, ξ_I^{abc} ,where a, b and c denote components along the cubic axes [100], [010] and [001] respectively. (Eq. 2 defines ξ_I with a different convention than Ref. 9, although the two conventions are equivalent for cubic materials in the independent particle approximation.)

Likewise, spin can also be optically injected into this sample. In our case, spin can be injected through one photon absorption of the 2ω pulse ($S_{2\omega}$), through two photon absorption of the ω pulse (S_ω), or through quantum interference between these two transition amplitudes (S_I). The total injection rate of spins aligned along the i direction is:

$$\dot{S}^i = \dot{S}^i_{2\omega} + \dot{S}^i_{\omega} + \dot{S}^i_{I} \,. \tag{3}$$

In order to separate the material properties from the optical fields, we introduce pseudotensors ζ_1, ζ_2 and ζ_I. The components of spin injected through one and two photon absorption alone are $\dot{S}^i_{2\omega} = \sum_{jk} \zeta_1^{ijk} E_{2\omega}^{j*} E_{2\omega}^{k}$ and $\dot{S}^i_{\omega} = \sum_{jklm} \zeta_2^{ijklm} E_{\omega}^{j*} E_{\omega}^{k*} E_{\omega}^{l} E_{\omega}^{m}$, respectively. The *spin control* components are

$$\dot{S}^i_{I} = \sum_{jkl} \zeta_I^{ijkl} E_{\omega}^{j*} E_{\omega}^{k*} E_{2\omega}^{l} + \text{c.c.} \,. \tag{4}$$

The spin control pseudotensor ζ_I is nonzero only in crystals that lack inversion symmetry. Since it is a fourth rank pseudotensor symmetric on its middle two indices, the spin control pseudotensor ζ_I is non-zero in crystals with zincblende symmetry, having two independent components: ζ_I^{abba} and ζ_I^{abab}. From a microscopic expression for ζ_I , one can show that it is purely imaginary in the independent particle approximation. We will assume this is valid in what follows, although it is a matter of convenience more than necessity since our experiment is not sensitive to the phase of ζ_I.

Population control (n_I) and spin control (S_I) signals will depend on the symmetry properties and the specific orientation of the semiconductor under study. For ω and 2ω at normal incidence on bulk (001)-oriented GaAs, n_I is zero [9] and S_I is restricted to lie in the (001) plane [10]; for other orientations, n_I can be nonzero, and S_I can be oriented along the propagation direction, z. (In this paper we limit the discussion to net spins with components along the $\pm z$-axis, as our measurement techniques are not sensitive to spins in the transverse plane.)

In the geometry we consider, 2ω and ω pulses propagate along the [111] direction (the z-axis) and are normally incident on the (111) plane of bulk GaAs, which can be rotated about the z-axis. The relevant crystal directions are shown in Fig. 1. As we will demonstrate below, both population and spin can be controlled in such a sample. The slowly varying fields are $\boldsymbol{E}_{2\omega} = |E_{2\omega}| \exp(i\phi_{2\omega})\, \hat{\boldsymbol{e}}_{2\omega}$ and $\boldsymbol{E}_{\omega} = |E_{\omega}| \exp(i\phi_{\omega})\, \hat{\boldsymbol{e}}_{\omega}$, where the 2ω and ω polarization unit vectors, $\hat{\boldsymbol{e}}_{2\omega}$ and $\hat{\boldsymbol{e}}_{\omega}$, lie in the (111) plane.

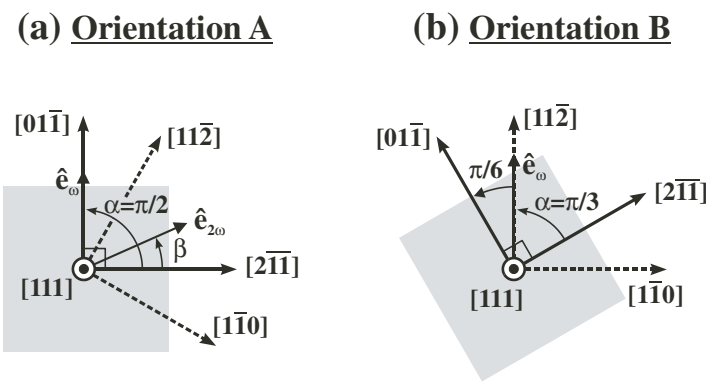

Fig. 1 Schematic of relevant crystallographic directions. Sample orientation B is achieved by rotating the sample $\pi/6$ about the z-axis from sample orientation A. Also shown are definitions of α and β referred to in Eqs. (5)–(6).

For linear polarizations, the carriers created through one- or two-photon absorption will have no net spin-polarization along the z-direction ($\dot{S}^z_{2\omega} = \dot{S}^z_{\omega} = 0$) [4, 10]. Conversely, when either pulse is circularly polarized and acting alone, carriers are injected with a net spin along the $+z$-direction for a left-circularly (σ^-) polarized 2ω or ω beam or with a net spin along the $-z$-direction for a right-circularly (σ^+) polarized 2ω or ω beam [4, 10].

For a fixed linearly or circularly polarized excitation field, the population injected by 2ω or ω acting independently does not depend on rotations of the sample about the z-axis [11]. The same is true for the spin. In contrast, the population control and spin control signals we demonstrate in this paper are strongly dependent on sample orientation.

3 Experimental technique To demonstrate population and spin control, we use the pump-probe geometry in Fig. 2. The ~100 fs fundamental pulse, with wavelength centered at 1.43 μm (the ω pulse), is generated in an optical parametric amplifier (OPA) that is pumped by a Ti:Sapphire-laser-seeded regenerative amplifier operating at 250 kHz. Second harmonic generation in BBO produces the 2ω pulse at 0.715 μm. The two pulses are temporally overlapped, propagate collinearly, and are focused at normal incidence onto a (111)-oriented bulk GaAs sample at room temperature. The phase difference $\Delta\phi \equiv 2\phi_\omega - \phi_{2\omega}$ is controlled with a scanning Michelson interferometer, and the polarization of each pulse is independently controlled with waveplates and polarizers, as shown in Fig. 2 (see Ref. 12 for more details).

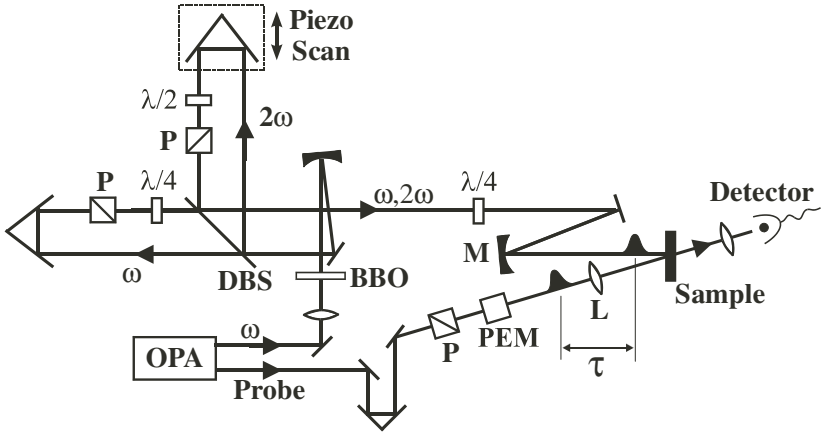

Fig. 2 Experimental geometry: BBO is used for second harmonic generation of ω into 2ω; DBS is a dichroic beamsplitter; P, $\lambda/2$ and $\lambda/4$ represent a polarizer, a half wave plate and a quarter wave plate, respectively; PEM is a photoelastic modulator used to modulate the probe polarization; L and M are a lens and a spherical curved mirror; τ is the time delay between pumps and probe.

A third pulse (at a wavelength of 0.81 μm and derived from the output of the regenerative amplifier after it has been used to pump the OPA) probes the population and spin of pump-injected carriers. The probe is spatially centered on the pump spots and arrives 0.9 ps after the pumps to allow for carrier thermalization.

The ~0.65 μm thick GaAs epilayer was grown on a (111)-oriented GaAs substrate, the substrate was removed with selective etching, and the epilayer was van der Waals bonded on a sapphire substrate to allow transmission measurements. This is the same sample used for the measurements in Ref. 9. The irradiances of the 2ω and ω pulses are ~160 MW/cm^2 and ~7.6 GW/cm^2, respectively. The pump photon energies are chosen to excite carriers out of the heavy hole and light hole valence bands, but not out of the split-off band. Carrier densities produced by the 2ω and ω pulses acting independently are approximately equal ($n_{2\omega} \cong n_{\omega} \cong 6 \times 10^{17}$ cm^{-3}); in a sense, balancing the two arms of our "matter interferometer". Although the two photon absorption coefficient differs for linearly and circularly polarized ω [11], we do not attempt to keep n_{ω} constant by adjusting the ω power, since the quantities we measure in this experiment are insensitive to the exact balance of $n_{2\omega}$ and n_{ω}.

To monitor the phase-dependent population change ($\Delta n = n(\Delta\phi) - n_0$, where $n_0 = n_{2\omega} + n_{\omega}$), we measure the differential transmission as a function of $\Delta\phi$ ($\Delta T(\Delta\phi)$) using a linearly polarized probe. A linearly polarized probe is equally sensitive to carriers with spins along $+z$ and $-z$; in this case, $\Delta T(\Delta\phi)$ is proportional to the phase-dependent change in total carrier density. This signal is normalized by the differential transmission induced by the average background carrier density, $n_0 \cong 1.2 \times 10^{18}$ cm^{-3}.

Alternatively, we use circular probe polarizations to monitor the spin control signal, since a σ^- (σ^+) polarized probe is more sensitive to the saturation of carriers with spins along $+z$ ($-z$) [4]. Because the probe propagates at a very small internal angle (~3°) with respect to normal incidence, the change in probe transmission is only sensitive to spins along $\pm z$. To measure the phase-dependent change in net spin along the z-axis ($\Delta S = S^z(\Delta\phi) - (S^z_{2\omega} + S^z_{\omega})$), we monitor $\Delta T(\Delta\phi)$ as the probe polarization is periodically modulated between σ^+ and σ^- polarizations with a photoelastic modulator (PEM). This measures the difference between $\Delta T(\Delta\phi)$ with a σ^+ probe and $\Delta T(\Delta\phi)$ with a σ^- probe, which is proportional to ΔS. This quantity is normalized by the differential transmission induced by the total spin injected when both 2ω and ω pulses are σ^- polarized, $S_0 = S^z_{2\omega(\sigma^-)} + S^z_{\omega(\sigma^-)}$.

4 Demonstration of population and spin control Figure 3a–b shows the results of measuring the phase-dependent change in population and spin at sample orientation A (see Fig. 1a). In Fig. 3a–b, both 2ω and ω beams are linearly polarized, and the ω polarization is along the $[01\bar{1}]$ direction ($\alpha = \pi/2$). In Fig. 3a, the 2ω beam is also along $[01\bar{1}]$ ($\beta = \pi/2$); in this case we see a strong spin control signal but little or no modulation of the population. By contrast, in Fig. 3b the 2ω beam is polarized orthogonal to the ω beam and lies along the $[2\bar{1}\bar{1}]$ direction ($\beta = 0$), allowing control of the population, but no discernable control of the spin. (The configuration of Fig. 3b repeats the sample orientation and polarization combination reported in Ref. 9, with similar results – both qualitatively and quantitatively – for Δn.) Therefore, at orientation A, parallel linear pump polarizations allow spin control without population control, whereas orthogonal polarizations allow population control without spin control.

Next we rotate the sample $\pi/6$ about the z-axis to sample orientation B (see Fig. 1b) so ω is polarized along $[11\bar{2}]$ ($\alpha = \pi/3$) and repeat the parallel and orthogonal linear polarization configurations. The results are shown in Fig. 3c-d. In contrast to the results at sample orientation A, for parallel linear excitation polarizations (now along $[11\bar{2}]$ ($\alpha = \beta = \pi/3$)), we observe population control but no discernable spin control. With orthogonal linear polarizations – ω along $[11\bar{2}]$ ($\alpha = \pi/3$), 2ω along $[1\bar{1}0]$ ($\beta = -\pi/6$) – we observe spin control but little or no population control. Therefore at sample orientation B, the dependences of the spin control and of the population control on the linear polarization combinations are reversed from the results at sample orientation A.

Thus for fixed parallel (or orthogonal) linear pump polarizations, the sample can first be oriented so that the phase $\Delta\phi$ can be used to control the spin, but not the population. The sample can then be rotated so that $\Delta\phi$ controls the population, but not the spin.

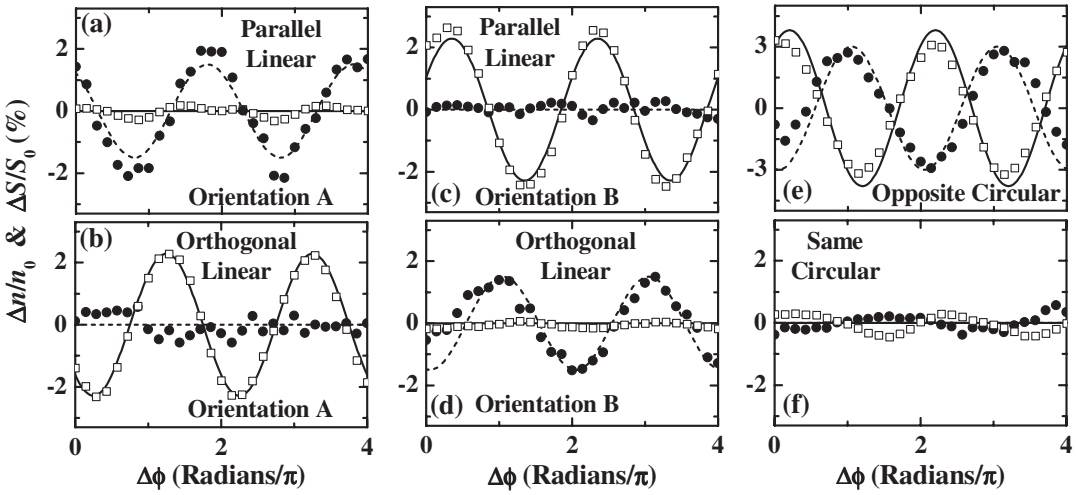

Fig. 3 Measured fractional change in spin (solid circles) and population (open squares) as a function of relative phase $\Delta\phi$ for various polarization combinations and sample orientations: (a) sample orientation A, parallel linear polarizations (along $[01\bar{1}]$), (b) orientation A, orthogonal linear polarizations (ω along $[01\bar{1}]$, 2ω along $[2\bar{1}\bar{1}]$), (c) orientation B, parallel linear polarizations (along $[11\bar{2}]$), (d) orientation B, orthogonal linear polarizations (ω along $[11\bar{2}]$, 2ω along $[1\bar{1}0]$), (e) opposite circular polarizations, and (f) same circular polarizations. Also shown are theoretical simulations of population control n_I/n_0 (solid lines) and spin control S_I^z/S_0 (dashed lines).

For *opposite circular* excitation, Fig. 3e shows that both the spin and the population are controlled simultaneously. Since the ω and 2ω circular polarizations have opposite handedness, the carriers injected by these two pulses have opposite net spin: the σ^+ polarized 2ω pulse injects carriers with a net spin along the $-z$-axis, while the σ^- polarized ω pulse injects carriers with net spin along the $+z$-axis. The magnitudes of the net spin injected per electron for one- and two-photon absorption are expected to be nearly equal [10], so that $\dot{S}^z_{2\omega} + \dot{S}^z_{\omega} \cong 0$, which we have verified experimentally by measuring the average background (non-phase-dependent) spin. Consequently, in the absence of spin control, there is approximately zero net spin along the z-direction, and the spin control signal causes the direction of the total $\dot{S}^z$ to oscillate between $+z$ and $-z$. By contrast, Fig. 3f shows that for *same circular* excitation, there is essentially no phase dependence to either population or spin injection, even though a highly spin-polarized background population is produced because $\dot{S}^z_{2\omega}$ and $\dot{S}^z_{\omega}$ both point along $+z$. In addition, we verified that the magnitudes of the $\Delta n/n_0$ and $\Delta S/S_0$ signals for same and opposite circular excitation do not depend on which sample orientation we choose, as expected from the theory (not shown).

Note that the relative phase of any two experimental curves cannot be deduced from the data in Fig. 3, since we did not verify whether there was interferometer drift between measurements taken under different experimental conditions such as different polarizations or sample orientations. We did, however, monitor the relative phase of differential transmission of the probe and 2ω beams as was done in Ref. 9; we found results consistent with the measurements reported in Ref. 9, which were performed in the same sample.

5 Macroscopic symmetry analysis We compare these experimental results with the macroscopic symmetry theory by deriving expressions for population and spin control signals appropriate to the polarization combinations and sample orientations used in Fig. 3. For the general case of ω and 2ω both linearly polarized at angles α and β with respect to the $[2\bar{1}\bar{1}]$ direction as shown in Fig. 1, Eq. (2) reduces to

$$\dot{n}_I = \frac{2\sqrt{2}}{\sqrt{3}} \xi_I^{abc} \left|E_{2\omega}\right| \left|E_{\omega}\right|^2 \cos\left(2\alpha + \beta\right) \cos\left(\Delta\phi\right), \tag{5}$$

where $\Delta\phi \equiv 2\phi_\omega - \phi_{2\omega}$, and we have assumed ξ_I^{abc} is real, as it is in the independent particle approximation [9]. For these same polarizations, the z-component of the spin control, from Eq. (4), is

$$\dot{S}_I^z = -\frac{1}{\sqrt{3}}\left(\mathrm{Im}\,\zeta_I^{abba} + 2\,\mathrm{Im}\,\zeta_I^{abab}\right)\left|E_{2\omega}\right|\left|E_\omega\right|^2 \sin\left(2\alpha+\beta\right)\sin\left(\Delta\phi\right). \tag{6}$$

Therefore, for the sample and polarization angles that yield a (negative or positive) maximum in the population control signal ($2\alpha+\beta = 0,\ \pi, \ldots$), the spin control along z will be zero. Likewise, when $\dot{S}_I^z$ is maximum ($2\alpha+\beta = \pi/2, 3\pi/2, \ldots$), n_I is zero. Indeed, this agrees with what we observe in Fig. 3a–d. When the angle between $\hat{\boldsymbol{e}}_{2\omega}$ and $\hat{\boldsymbol{e}}_\omega$ is fixed and the sample is rotated about the z-axis, the magnitudes of $\dot{n}_I$ and $\dot{S}_I^z$ have 6-fold rotational symmetry. As a result, when 2ω and ω have parallel linear polarizations ($\alpha = \beta$), $\dot{n}_I \propto \cos(3\alpha)$ and n_I is maximized at $\alpha = 0, \pi/3, 2\pi/3$, etc. Thus the population control signal with parallel linear polarizations is maximum if $\hat{\mathbf{e}}_{2\omega}$ and $\hat{\mathbf{e}}_\omega$ lie along any of the $\langle 2\bar{1}\bar{1}\rangle$ family of directions, whereas it is zero if $\hat{\boldsymbol{e}}_{2\omega}$ and $\hat{\boldsymbol{e}}_\omega$ are parallel along any of the $\langle 1\bar{1}0\rangle$ directions.

If ω and 2ω are both circularly polarized, the prediction is quite different. When the beams have opposite circular polarizations (2ω is σ^+ and ω is σ^-), Eqs. (2) and (4) simplify to give the population control

$$\dot{n}_I = \frac{4}{\sqrt{3}}\,\xi_I^{abc}\left|E_{2\omega}\right|\left|E_\omega\right|^2 \cos\left(\Delta\phi\right) \tag{7}$$

and the z-component of spin control

$$\dot{S}_I^z = \frac{2}{\sqrt{3}}\left(\mathrm{Im}\,\zeta_I^{abba} + 2\,\mathrm{Im}\,\zeta_I^{abab}\right)\left|E_{2\omega}\right|\left|E_\omega\right|^2 \cos\left(\Delta\phi\right). \tag{8}$$

Conversely, when ω and 2ω have the *same* circular polarization, both $\dot{S}_I^z$ and n_I should be zero. The magnitudes of population and spin control signals for same and opposite circular excitation should be independent of sample orientation; this is intuitively satisfying, because circularly polarized light does not have a preferred direction in the transverse plane (as linearly or elliptically polarized light does). Note that although the spin control tensor has two independent components, our experiment can only measure the sum ($\mathrm{Im}\,\xi_I^{abba} + 2\,\mathrm{Im}\,\xi_I^{abab}$); it is not sensitive to their relative magnitudes. These relative magnitudes could be measured with normal incidence on a (110)-oriented surface.

At the electric field strengths that balance one- and two-photon absorption rates, for linear polarizations

$$\frac{\dot{n}_I}{\dot{n}_{2\omega}+\dot{n}_\omega} = \sqrt{\frac{2}{3}}\,\frac{\xi_I^{abc}}{\sqrt{\xi_1^{aa}\,\xi_2^{aaaa}\left(1-\sigma/2\right)}}\cos\left(2\alpha+\beta\right)\cos\left(\Delta\phi\right), \tag{9}$$

where σ is the two photon absorption anisotropy parameter [11], and for opposite circular polarizations

$$\frac{\dot{n}_I}{\dot{n}_{2\omega}+\dot{n}_\omega} = \frac{2}{\sqrt{3}}\,\frac{\xi_I^{abc}}{\sqrt{\xi_1^{aa}\,\xi_2^{aaaa}\left(1-\sigma/6-\delta/2\right)}}\cos\left(\Delta\phi\right), \tag{10}$$

where δ is the two photon absorption circular dichroism parameter [13].

The solid lines in Fig. 3 are plots of $\dot{n}_I/(\dot{n}_{2\omega}+\dot{n}_\omega)$ using Eq. (9) for (a–d) and using Eq. (10) for (e). These simulations have been shifted along the $\Delta\phi$-axis to line up with the data, to show that the magnitudes of the simulations are in good quantitative agreement with the data. The single value of 3.2% was chosen for $\xi_I^{abc}\Big/\sqrt{\xi_1^{aa}\,\xi_2^{aaaa}}$ to give the best fit to all population control data, while values of σ and δ were taken from a 14-band model calculation [13].

The dashed lines in Fig. 3 are plots of $\dot{S}_I^z/(\dot{S}_{2\omega(\sigma-)}^z + \dot{S}_{\omega(\sigma-)}^z)$ using Eq. (6) for (a–d), and Eq. (8) for (e). The simulations were again shifted along the $\Delta\phi$-axis, and the single value of 2.6% for $(\mathrm{Im}\,\zeta_I^{abba} + 2\,\mathrm{Im}\,\zeta_I^{abab})\,|E_{2\omega}|\,|E_\omega|^2/(\dot{S}_{2\omega(\sigma-)}^z + \dot{S}_{\omega(\sigma-)}^z)$ was chosen to give the best fit to all the data; again, there is good quantitative agreement between data and theory.

Our measured value of the population control ratio with a 715 nm 2ω pulse is close to the value measured by Fraser et al. with a 775 nm 2ω pulse in this same sample [9]. A population control ratio of a few percent is expected, since the effect only exists as a result of the lack of inversion symmetry; indeed, *ab initio* calculations indicate that $\xi_1^{abc} \Big/ \sqrt{\xi_1^{aa}\,\xi_2^{aaaa}}$ is 6.4% at these wavelengths [9]. Our experimental fit value is smaller by a factor of two, similar to the result in Ref. 9; much of the difference between data and theory can be attributed to the use of a relatively thick sample [9]. Similar arguments could be made for the magnitude of the spin control ratio: it too relies on the lack of inversion symmetry. One can take the population control ratio as a rough upper bound on the spin control ratio; from this point of view, the spin control ratio we have measured is in line with our expectations.

In contrast to the work reported in this paper, we recently demonstrated two-color quantum interference control of ballistic spin *currents* in (001)-oriented GaAs [12]. Due to the symmetry of (001)-GaAs, we did not expect to observe coherent control of the overall carrier population [8, 9] or spin [10]. The measurements performed in Ref. 12 – electrical detection of currents through charge collection with electrodes – were not sensitive to overall carrier population or spin.

6 Conclusion We have demonstrated that quantum interference allows the use of the phase together with the polarization of the light and the crystallographic symmetry to independently control either the spin or the carrier population or both. Specifically, we have shown: (i) For a selected fixed sample orientation and linearly polarized ω and 2ω pulses, parallel polarizations allow the control of the population without modulating the spin; conversely, orthogonal linear polarizations allow the control of the spin, but not the population. (ii) When the sample is rotated $\pi/6$ about the z-axis, the dependences of the spin control and of the population control on these polarizations are reversed. (iii) For opposite circular polarizations, both the spin and the population can be simultaneously controlled, regardless of sample orientation. (iv) When ω and 2ω have the same circular polarization, $\Delta\phi$ controls neither the spin nor the population. We have also shown that all results agree qualitatively with a theory based on macroscopic symmetry analysis.

Acknowledgements We thank Eric Gansen, Scot Hawkins, Xinyu Pan, Petr Nemec and Yaser Kerachian for insightful conversations. This work was supported in part by the Office of Naval Research, the Defense Advanced Research Projects Agency, Photonics Research Ontario and the Natural Science and Engineering Research Council of Canada.

References

[1] A. P. Heberle, J. J. Baumberg, E. Binder, T. Kuhn, K. Köhler and K. H. Ploog, IEEE J. Sel. Top. Quantum Electron. **2**, 769 (1996).
[2] X. Marie, P. Le Jeune, T. Amand, M. Broussear, J. Barrau, M. Paillard and R. Planel, Phys. Rev. Lett. **79**, 3222 (1997).
[3] N. H. Bonadeo, J. Erland, D. Gammon, D. Park, D. S. Katzer, and D. G. Steel, Science **282**, 1473 (1998).
[4] F. Meier and B. P. Zakharchenya, Eds., Optical Orientation, Modern Problems in Condensed Matter Sciences Vol. 8 (North-Holland, Amsterdam, 1984).
[5] S. A. Wolf, D. D. Awschalom, R. A. Buhrman, J. M. Daughton, S. von Molnár, M. L. Roukes, A. Y. Chtchelkanova and D. M. Treger, Science **294**, 1488 (2001) and references therein.
[6] D. D. Awschalom, D. Loss, and N. Samarth, Eds., Semiconductor Spintronics and Quantum Computation (Springer-Verlag, Heidelberg, 2002) and references therein.
[7] J. A. Gupta, R. Knobel, N. Samarth, and D. D. Awschalom, Science **292**, 2458 (2001).
[8] H. M. van Driel and J. E. Sipe, in: Ultrafast Phenomena in Semiconductors, edited by K.-T. Tsen (Springer-Verlag, New York, 2001), pp. 261–307 and references therein.
[9] J. M. Fraser, A. I. Shkrebtii, J.E. Sipe and H.M. van Driel, Phys. Rev. Lett. **83**, 4192 (1999).
[10] R. D. R. Bhat and J. E. Sipe, Phys. Rev. Lett. **85** 5432 (2000).
[11] M. D. Dvorak, W. A. Schroeder, D. R. Andersen, A. L. Smirl, and B. S. Wherrett, IEEE J. Quantum Electron. **30**, 256 (1994).
[12] M. J. Stevens, A. L. Smirl, R. D. R. Bhat, J. E. Sipe, and H. M. van Driel, J. Appl. Phys. **91**, 4382 (2002).
[13] D. C. Hutchings and B. S. Wherrett, Phys. Rev. B **49**, 2418 (1994).